Evidence of an Odorant-Binding Protein in the Human Olfactory Mucus: Location, Structural Characterization, and Odorant-Binding Properties†

Loïc Briand,‡ Corinne Eloit,§,|| Claude Nespoulous,‡ Valérie Bézirard,‡ Jean-Claude Huet,‡ Céline Henry,‡ Florence Blon,‡ Didier Trotier,|| and Jean-Claude Pernollet*,‡

Biochimie et Structure des Protéines, Unité de recherches INRA 477, Domaine de Vilvert, F-78352, Jouy-en-Josas Cedex, France, Département O.R.L., Hôpital Lariboisière, 2 Rue Ambroise Paré, F-75010 Paris, France, Neurobiologie sensorielle, Ecole Pratique des Hautes Etudes, 1 Avenue des Olympiades, F-91305 Massy and Physiologie Oro-faciale, JE359, Université Paris 7, 2 Place Jussieu, F-75251 Paris, France

Received November 6, 2001; Revised Manuscript Received February 21, 2002

ABSTRACT: Odorant-binding proteins (OBPs) are small abundant extracellular proteins belonging to the lipocalin superfamily. They are thought to participate in perireceptor events of odor detection by carrying, deactivating, and/or selecting odorant molecules. Putative human OBP genes (*hOBP*) have recently been described [Lacazette et al. (2000) *Hum. Mol. Genet. 9*, 289−301], but the presence of the corresponding proteins remained to be established in the human olfactory mucus. This paper reports the first evidence of such expression in the mucus covering the olfactory cleft, where the sensory olfactory epithelium is located. On the contrary, hOBPs were not observed in the nasal mucus covering the septum and the lower turbinate. To demonstrate the odorant binding activity of these proteins, a corresponding recombinant protein variant, $hOBP_{IIa\alpha}$, was secreted by the yeast *Pichia pastoris* and thoroughly characterized. It appears as a monomer with one disulfide bond located between C59 and C151, a conservative feature of all other vertebrate OBPs. By measuring the displacement of several fluorescent probes, we show that $hOBP_{IIa\alpha}$ is able to bind numerous odorants of diverse chemical structures, with a higher affinity for aldehydes and large fatty acids. A computed 3D model of $hOBP_{IIa\alpha}$ is proposed and reveals that two lysyl residues of the binding pocket may account for the increased affinity for aldehydes. The relatively limited specificity of $hOBP_{IIa\alpha}$ suggests that other human OBPs are expected to take into account the large diversity of odorant molecules.

To reach their membrane receptors embedded in the membrane of the olfactory neurons, airborne odorants, which are commonly hydrophobic molecules, have to be conveyed through the aqueous nasal mucus. The odorant-binding proteins (OBPs)[1], which are abundant low-molecular-weight soluble proteins (around 20 kDa) secreted by the olfactory epithelium in the nasal mucus of vertebrates, are candidates for playing a carrier role (*1*). These proteins reversibly bind odorants with dissociation constants in the micromolar range. Although their functions are still unclear, OBPs are also suspected to participate in the deactivation of odorants (*2*). Vertebrate OBPs belong to the lipocalin superfamily (*3*, *4*). Although members of this superfamily display low sequence similarity (usually lower than 20% amino acid identity), all share a conserved folding pattern, an 8-stranded β-barrel flanked by an α-helix at the C-terminal end of the polypeptide chain. The β-barrel defines a central apolar cavity, called calix, whose role is to bind and transport hydrophobic odorant molecules (*5*−*7*). OBPs have been identified in a variety of species, including cow, pig, rabbit, mouse, and rat (*8*−*13*) since the discovery of the first vertebrate OBP isolated from the bovine nasal mucus (*14*, *15*). Different OBP subtypes have been reported to simultaneously occur in the same animal species, three in pig (*8*, *16*), four in mouse (*17*−*19*), three in rat (*12*, *13*, *20*−*23*), three in rabbit (*24*), and at

† This work was supported by the French Institut National de la Recherche Agronomique and by the Association pour la Recherche sur le Cancer.

* Corresponding author: Phone 33 1 34 65 27 50; Fax 33 1 34 65 27 65; E-mail: pernolle@jouy.inra.fr.

‡ Biochimie et Structure des Protéines.

§ Département O.R.L., Hôpital Lariboisière.

|| Neurobiologie sensorielle et Physiologie Oro-faciale.

[1] Abbreviations: 1,8-ANS, 8-anilino-1-naphthalenesulfonic acid; 1-AMA, 1-aminoanthracene; ASA, (±)-12-(9-anthroyloxy)stearic acid; BrC12-Ac, 12-bromododecanoic acid; BrC15-Ac, 15-bromopentadecanoic acid; CD, circular dichroism; α-CHCA, α-cyano-4-hydroxycinnamic acid; CH_3CN, acetonitrile; CNBr, cyanogen bromide; citralva, 3,7-dimethyl-2,6-octadienenitrile; citronellal, (±)-3,7-dimethyl-6-octen-1-al; citronellol, (±)-3,7-dimethyl-6-octen-1-ol; DACA, dansyl-DL-α-aminocaprylic acid; DAUDA, 11-((5-(dimethylaminonaphthalenyl-1-sulfonyl)amino)undecanoic acid; DHB, 2,5-dihydroxybenzoic acid; eugenol, 2-methoxy-4-(2-propenyl)phenol; EDTA, ethylenediaminetetraacetic acid; γ-decalactone, gamma-*n*-hexyl-gamma-butyrolactone; geraniol, 2-*trans*-3,7-dimethyl-2,6-octadien-1-ol; helional, α-methyl-3,4-methylene-dioxy hydro-cinnamic aldehyde; hOBP, human odorant-binding protein; HPLC, high performance liquid chromatography; IBMP, 2-isobutyl-3-methoxypyrazine; β-ionone, 4-(2,6,6-trimethyl-1-cyclohexen-1-yl)-3-buten-2-one); lilial, 2-methyl-3-(4-*tert*-butylphenyl)-propanal; MALDI, matrix-assisted laser desorption ionization mass spectrometry; TOF, time-of-flight; Mut^s, MeOH utilization slow; NPN, *N*-phenyl-1-naphthylamine; OBP, odorant-binding protein; α-pinene, (1*S*,5*S*)-2,6,6-trimethyl bicyclo-[3.1.1]-2-heptene; PTH, phenyl thiohydantoyl; QAE, quaternary amino ethyl; RPLC, reversed phase liquid chromatography; SDS−PAGE, sodium dodecyl sulfate−polyacrylamide gel electrophoresis; TFA, trifluoroacetic acid; vanillin, 4-hydroxy-3-methoxybenzaldehyde.

10.1021/bi015916c CCC: $22.00
Published on Web 05/15/2002

least eight in porcupine (*25*, *26*). Their binding properties, investigated in rat, demonstrated that the three OBPs are specially tuned toward distinct chemical classes of odorants (*27*). Rat OBP-1 preferentially binds heterocyclic compounds such as pyrazine derivatives (*13*, *28*), and OBP-2 appears to be more specific for long-chain aliphatic aldehydes and carboxylic acids (*28*), whereas OBP-3 was described to interact strongly with odorants composed of saturated or unsaturated ring structure (*23*).

Various proteins have been detected in human nasal mucus including a protein with N-terminal identical to tear lipocalin (*29*−*33*). However, contrary to all other vertebrates so far studied, the presence of OBP-like proteins in the olfactory mucus has not yet been observed in humans. Recently, two putative human OBP genes (*hOBP$_{IIa}$* and *hOBP$_{IIb}$*) localized on chromosome 9q34 have been described (*34*). The *hOBP$_{IIa}$* gene codes for a protein 45.5% homologous to rat OBP-2 and is transcribed in the nose, as opposed to *hOBP$_{IIb}$*, transcribed in the genital sphere and coding for a protein 43% identical to the human tear lipocalin. Alternatively, spliced mRNAs have been observed for both genes generating proteins with different C-termini. Nevertheless, the capability of putative proteins corresponding to the *hOBP$_{IIa}$* gene to bind odorants is still questionable.

Here we report protein investigations of the mucus covering different areas of the human nasal cavity, which led us to identify OBPs specifically found in the mucus of the olfactory cleft. Using the yeast *Pichia pastoris*, we then expressed the alternatively spliced isoform hOBP$_{IIa\alpha}$, which was thoroughly characterized as a functional protein. In addition, we examined the selectivity of binding of this human OBP using a vast array of odorants and long chain fatty acids.

EXPERIMENTAL PROCEDURES

Nasal Mucus Sampling. Samples of nasal mucus (~4 μL) were obtained using a sterile polyethylene catheter (Merck-Boiron, France, 0.7-mm internal diameter, 1.09-mm external diameter, 100-mm in length) connected to a 20 μL Gilson Pipetman. Sampling was performed on healthy adult volunteers lying supine in a quiet room. Although it was painless and did not present inherent risk, the sampling procedure was performed according to the recommendations from the Declaration of Helsinki (DHEW Publication, NIH 86-23) for nontherapeutic clinical research: samplings were performed by a ENT medical surgeon (CE) who fully informed the subjects about the nature, the purpose, and the potential risks. Subjects afterward gave their free consent. Under optical control with an endoscope (Storz Foreward Endoscope 0°, 4-mm external diameter supplied with a cold light), the catheter was gently introduced into the nasal cavity. Human olfactory epithelium covers a surface of about 100−400 mm^2 in the uppermost part of the nasal cavity, named the olfactory cleft, which is not directly visible using an endoscope, except in its most anterior part, above the middle turbinate (*35*). We therefore sampled the olfactory mucus at this level by locating the tip of the catheter above the middle turbinate (Figure 1). To avoid an awkward feeling for the volunteers, the sampling was performed after a slight anesthesia of the nasal cavity with a puff of lidocaine chlorhydrate (Astra, France). Nasal mucus was also sampled on the inferior turbinate and the anteroinferior part of the septum, with no need of anesthesia. All mucus samples were immediately frozen in liquid nitrogen and kept at −20 °C until use.

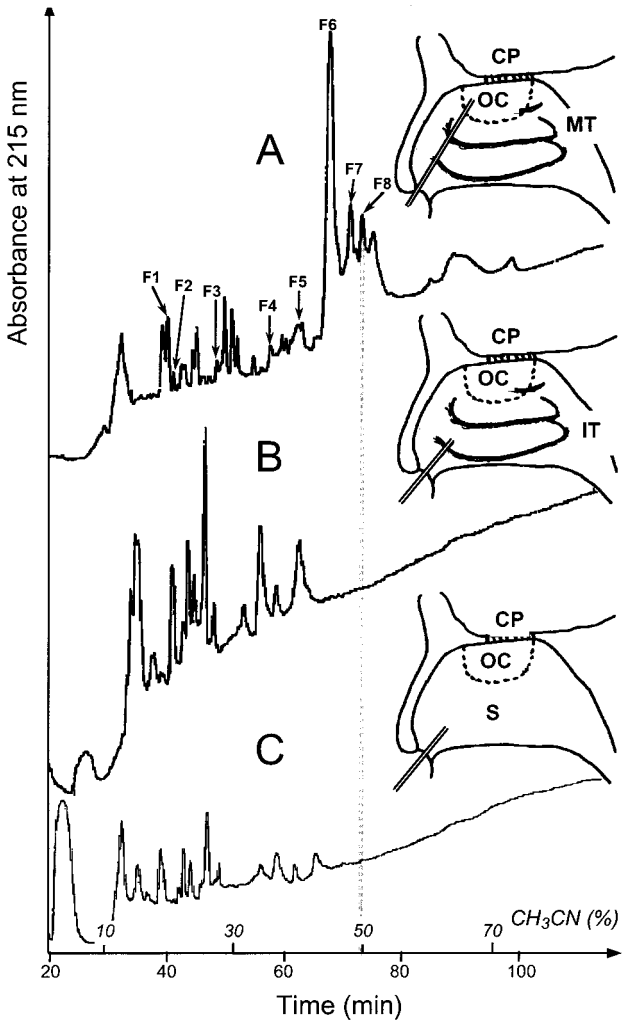

FIGURE 1: Reversed-phase liquid chromatography of nasal mucus sampled at various levels of the human nasal cavity. (A) Olfactory cleft sample; (B) inferior turbinate sample; (C) septum sample. Schematic drawings (adapted from ref *54*) indicating the approximate location of the catheter tip (parallel lines) during mucus sampling at the level of the olfactory cleft (in panel A, lateral side of the nasal cavity), the anterior part of the inferior turbinate (in panel B, lateral side of the nasal cavity), and the septum (in panel C, medial side of the nasal cavity); CP, cribriform plate; IT, inferior turbinate; MT, middle turbinate; OC, approximate location of the sensory olfactory cleft; S, septum. Fractions that are named in panel A contained proteins identified in data libraries using N-terminal sequences. The grayed vertical bar shows the position of the peak in which sequences have been observed to correspond to human putative OBPs. The abscissa axis indicates both elution time and the corresponding CH_3CN percentage.

Reversed Phase High Performance Liquid Chromatography. Samples (~4 μL), contained in a catheter, were diluted to 20 μL by solvent A (0.1% v/v formic acid (Fluka) and 4 mM ammonium acetate (Fluka) in water). RPLC was run with an Applied Biosystems device (pump 140D and UV detector 785 with U-shaped fused silica tubing, 7-mm path length) on a C4 LC−Packings capillary column (0.3 × 150-mm, 300 Å) at controlled temperature (40 °C). The gradient was made by mixing solvent A with solvent B (90% CH_3-CN, 0.1% v/v formic acid, and 4 mM ammonium acetate in water) at a flow rate of 4 μL/min. The CH_3CN gradient began

at 4.5% and increased linearly to 85.5% in 90 min. The flow was monitored by spectrophotometry at 215 nm, and fractions were manually collected.

Sequencing and Mass Spectrometry. N-terminal amino acid sequence analyses were performed by automated Edman chemistry using a Perkin-Elmer Procise 494 HT protein sequencer with methods and reagents of the manufacturer. One microliter of RPLC fractions was mixed on the stainless steel MALDI plate with 1 μL of DHB (Aldrich) (10 mg/mL in 50% CH_3CN, 0.15% v/v TFA) and dried at room temperature. Mass spectra were acquired on a Voyager DE-STR$^+$ time-of-flight mass spectrometer (Applied Biosystems) equipped with a nitrogen laser emitting at 337 nm. Spectra were recorded in positive linear mode with 25 kV as accelerating voltage, a delayed extraction time of 1200 ns, and a 94% grid voltage. The spectra were externally calibrated using a mix composed by horse heart cytochrome C $(M + H)^+ = 12\,361.1$ Da, horse apomyoglobin $(M + H)^+ = 16\,952.6$ Da, and bovine carbonic anhydrase $(M + H)^+ = 29\,024$ Da. Proteins were identified by a search in amino acid sequence databases, NCBInr.8.22.2001, Genpept.8.26.2001, and SwissProt.8.20.2001 by means of MS-Pattern (2.4.1) search engine (http://prospector.ucsf.edu/). No restriction was used for either proteins or species, while a single amino acid substitution was allowed. HPLC grade water (Merck), analytical grade TFA, CH_3CN, and MeOH (Applied Biosytems) were used for mass spectrometry analysis and preparation of digests.

Strains and Materials. *Escherichia coli* strain DH5α was used for DNA subcloning and propagation of the recombinant plasmid. *Pichia pastoris* strain GS115 (*his*4) was used in the expression study. Oligonucleotides were synthesized by MGW Biotech (France). pPIC9K was purchased from Invitrogen (France). IBMP, eugenol, *2*-octanone, octanoic acid, citronellol, and octane were obtained from Acros Organics (France). 3,7-Dimethyloctanal, nonanal, and lilial were kindly provided by Givaudan-Roure (Allauch, France). Citralva, helional, and γ-decalactone were gifts from International Flavors and Fragrances (Dijon, France), Floressence (Courbevoie, France), and SKW Biosystems (Grasse, France), respectively. All other odorants, fatty acids, and chemicals were provided by Sigma (France). Origins of other chemicals are indicated in the text.

Gene Synthesis and Construction of the Expression Vector. A gene encoding $hOBP_{IIa\alpha}$ (GenBank #AJ251021) was synthesized by Integrated DNA Technologies, Inc. (USA), with codons optimized for expression in *Saccharomyces cerevisiae*, from overlapping oligonucleotides into the pCRII TOPO TA vector (Promega). The construct was then subcloned into the *Sac*I and *Eco*RI sites of pPIC9K, generating the plasmid pPIC9K-$hOBP_{IIa\alpha}$ with the prepro-sequence of the α mating-factor without the EAEA repeat between the α mating-factor secretion peptide and the mature hOBP sequence. The construct was confirmed by DNA sequencing using an ABI Prism 310 sequencer (PE Biosystems, France).

Transformation of Pichia pastoris and Screening for OBP Expression. The expression plasmid was linearized with *Bgl*II and later transferred into the *Pichia pastoris* yeast host through electroporating method as described in the manual (version 3.0) of the *Pichia* expression kit (Invitrogen). The selection of multicopy integrants has been made using increased levels of G418 (Clontech, Ozyme, France). Large scale production were achieved as recently described (*13*) except that the protein was secreted for only 3 days using buffered minimal MeOH medium at pH 8.0 supplemented with 2% tryptone (Sigma) and 5 mM EDTA. During the induction period, MeOH was fed twice a day to maintain a concentration of 0.5% v/v.

Purification of the Recombinant OBP. The supernatant was chilled and clarified by centrifugation at 6000*g* for 30 min at 4 °C and by filtration (0.22 μm). The solution was then dialyzed against water for 1 day at 4 °C, using a dialysis tube with a 12 000−14 000 Da cut off (Spectrapor, Polylabo, France) and subsequently for 3 days against 0.1% v/v acetic acid solution. Precipitated $hOBP_{IIa\alpha}$ was resuspended in 50 mM potassium phosphate buffer, pH 7.5, and loaded on anion-exchange chromatography column using a Vydac QAE column (300 VHP, 7.5 mm i.d. × 50 mm, Interchim, France) equilibrated with 50 mM potassium phosphate buffer, pH 7.5. The flow rate was 1 mL/min, and the absorbance was recorded at 275 nm. Unbound fractions containing $hOBP_{IIa\alpha}$ were analyzed by SDS−PAGE, pooled, and stored at −20 °C.

Recombinant OBP Characterization. SDS−PAGE (16% acrylamide) was performed using a Mini-Protean II system (Bio-Rad, France) (*36*). The molecular weight calibration kits LMW and PMW (Pharmacia, France) were used, and the proteins were stained with Serva blue G. MALDI-TOF was performed in the same conditions as for the mucus analysis. Oligomerization of the undenatured recombinant protein was studied by exclusion-diffusion chromatography on a 24-mL bed volume Superose 12 column (Pharmacia). The column was equilibrated in 100 mM potassium phosphate, pH 7.5, 150 mM NaCl, at 0.2 mL/min. Bovine serum albumin (67 kDa), chicken egg ovalbumin (43 kDa), dimeric bovine β-lactoglobulin (36 kDa), bovine carbonic anhydrase (30 kDa), soybean trypsin inhibitor (21.5 kDa), and bovine ribonuclease A (13.7 kDa), purchased from Sigma, were employed as standards. A 100-μL sample of purified $hOBP_{IIa\alpha}$ was loaded at 0.5 mg/mL onto the Superose column, and the elution profiles were obtained from on-line UV detection at 280 nm. CD spectra were recorded using a JASCO J-810 spectropolarimeter and analyzed as previously described (*37*). $hOBP_{IIa\alpha}$ concentrations were determined using UV spectroscopy employing the extinction coefficient of 14 245 M^{-1} cm^{-1} at 276.0 nm, calculated according to ref *38*. Protein samples (about 1 mg/mL in 50 mM potassium phosphate buffer, pH 7.0) were placed in a 0.01-cm path length cell. Baseline was recorded with phosphate buffer. Secondary structure proportions were computed with the algorithm of Deleage and Geourjon (*39*).

Peptide Mapping and Disulfide Bridge Assignment. To determine the disulfide bridge pairing, 1 nmol of lyophilized unreduced $hOBP_{IIa\alpha}$ was dissolved in 40 μL of Fluka CNBr (22 mg/mL) in 70% v/v TFA, incubated in the dark for 24 h at room temperature. The sample was diluted twice with water and then dried by centrifugation in a vacuum. TFA (10 μL) was added to the sample for 1 h incubation in the dark at room temperature and dried again. The sample was recovered in 50 μL of 20% v/v CH_3CN. Five microliters of sample diluted to 10 μL with solvent A (described above) was then submitted to RPLC in the same conditions as those used for the mucus analysis. Resulting peptides were

analyzed by MALDI-TOF mass spectrometry using the same apparatus as above, but with different conditions. A 0.5-μL aliquot was spotted directly onto the MALDI sample plate, dried at room temperature before adding 0.5 μL aliquot of the matrix solution (3 mg/mL of Aldrich α-CHCA in 50% CH_3CN with 0.1% v/v TFA) prepared daily. For large peptides, we also used DHB as matrix by directly mixing samples and matrix solution onto the MALDI plate. The accelerating voltage used was 20 kV. Spectra were recorded in positive reflector mode with a delayed extraction time of 130 ns and a 62% grid voltage. In some cases, spectra were recorded in positive linear mode with a delayed extraction time of 250 ns, an accelerating voltage of 25 kV, and a 94% grid voltage. Spectra were calibrated using an external calibration composed by des-Arg1-bradykinin $(M + H)^+$= 904.4681 Da, human angiotensin I $(M + H)^+ = 1296.6853$ Da, neurotensin $(M + H)^+ = 1672.9175$ Da, melittin from bee venom $(M + H)^+ = 2845.762$ Da, and bovine insulin B chain disulfonate $(M + H)^+$= 3494.6513 Da. All values refer to monoisotopic ions, as those reported below.

To investigate possible artifactual posttranslational modifications of the recombinant protein, a tryptic digestion of $hOBP_{IIa\alpha}$ was achieved as already described (*40*). One nmole of protein in 50 μL of 50 mM potassium phosphate buffer pH 7.5 was adsorbed on a Prosorb PVDF membrane (Applied Biosystems, France) and washed twice with 10% v/v MeOH (100 μL) before being dried. The membrane was cut off with a punch prior treatment. For reduction and alkylation, PVDF membrane was wetted with 5 μL of MeOH. The protein was reduced with 20 mM dithiothreitol (Serva, France) in 100 μL of 67 mM Tris-HCl, 0.7 mM EDTA pH 8.4 and 6 M guanidine hydrochloride (Fluka, France) for 2 h at 40 °C and then alkylated with 50 mM iodoacetamide (Sigma) for 1 h at room temperature in the dark. Alkylation was halted by addition of 2% v/v 2-mercaptoethanol (Sigma). The membrane was washed 5 times with 10% v/v MeOH (400 μL) to eliminate salts and reagents, and then dried at room temperature and cut in two halves.

For trypsin (EC.3.4.21.4) digestion, one-half of the membrane was cut into small pieces. The digestion was performed on reduced and alkylated protein in 10 μL of 50 mM ammonium bicarbonate pH 8.0 and 2 μL of 0.25 μg/μL of modified trypsin (Promega, sequencing grade) for 18 h in a thermomixer (Eppendorf) at 37 °C and 500 rpm. The supernatant and two washes of the membrane with 5% v/v TFA and one further wash with 100% TFA were dried by centrifugation in a vacuum. The sample was dissolved with 10 μL of 0.1% v/v TFA for mass spectrometry. MALDI-TOF was performed using internal calibration with two peptides originating from trypsin autolysis, $(M + H)^+$ 2211.1040 and 842.5090 *m/z*.

Fluorescence-Based Ligand Binding. The fluorescent probes 1,8-ANS and 1-AMA were from Fluka (France). NPN was purchased from Acros Organics (France). DAUDA was provided by Molecular Probes (Eugene, OR). DACA and ASA were from Sigma (France). BrC12-Ac and BrC15-Ac were purchased from Aldrich (France) and Fluka (France), respectively. Fluorophore ligand binding experiments were performed with 2 μM $hOBP_{IIa\alpha}$ solutions in 50 mM potassium phosphate buffer, pH 7.5. The concentration of $hOBP_{IIa\alpha}$ was determined by quantitative amino acid analysis of the recombinant protein. The fluorescent probes were dissolved in 10% v/v MeOH as 1 mM stock solution. Successive 1-μL fluorescent probe aliquots were added to 1 mL of $hOBP_{IIa\alpha}$ solution. Spectra were recorded at 25 °C using a SFM 25 Kontron fluorometer with a 5-nm bandwidth for both excitation and emission. No cut off filter was used in the excitation beam. The excitation wavelengths used for DAUDA, DACA, ASA, 1-AMA, 1,8-ANS, and NPN were 345, 345, 360, 290, 372, and 337 nm, respectively. Once the binding equilibrium has been reached, in about 1 min as verified by time course experiments (not shown), the relative proportion of probe bound to $hOBP_{IIa\alpha}$ was calculated by measuring fluorescence emission (expressed in arbitrary units). Dissociation constants (K_d) were calculated from a plot of fluorescence intensity versus concentration of free ligand, obtained with a standard nonlinear regression method (*41*) using Deltagraph 4.5 software.

The competitive binding assays aimed to displace the probes with ligands were performed with 2 μM of $hOBP_{IIa\alpha}$ in 50 mM potassium phosphate buffer, pH 7.5 with 3 and 5 μM probe concentrations for DAUDA and NPN, respectively. To prevent artifactual solvent binding (*13*), the competitor odorants and fatty acids were dissolved in 10% v/v MeOH and 100% MeOH, respectively. Competitor concentrations causing a fluorescence decay to half-maximal intensity were taken as IC_{50} values. The apparent K_{diss} values were calculated as $K_{diss} = [IC_{50}]/(1 + [L]/K_d)$ with [L] being the free fluorophore concentration and K_d being the OBP−fluorophore complex dissociation constant (*42*). In addition, we tested tryptophan intrinsic fluorescence quenching using brominated C12 and C15 fatty acids. BrC12-Ac and BrC15-Ac were weighed and dissolved in 100% MeOH as 1 mM stock solutions. Tryptophan fluorescence was determined using an excitation wavelength of 285 nm and an emission wavelength of 325 nm with 2 μM of $hOBP_{IIa\alpha}$ in 50 mM potassium phosphate buffer, pH 7.5.

3D Structure Modeling. The tertiary structure predictions of $hOBP_{IIa\alpha}$, human tear lipocalin, and rat OBP-2 were obtained using the automated comparative protein modeling server http://www.expasy.ch/swissmod/SWISS-MODEL.html (*43*), after multiple alignments with sequences of lipocalins of known 3D structures. The major horse allergen (PDB accession number 1EW3A.pdb) was used as a matrix for the three proteins; tear lipocalin modeling was simultaneously performed with the major horse allergen and bovine β-lactoglobulin (PDB accession numbers: 1B0O.pdb, 1BEBA.pdb, 1BEBB.pdb, 1B8EA.pdb, and 1BSQA.pdb). Molecular surface was calculated using the Connolly algorithm included in the Insight II package (Accelrys) with a probe radius of 1.4 Å.

RESULTS

Protein Content of Nasal Mucus. We analyzed the protein content of nasal mucus using a classical high performance liquid chromatography approach, which already permitted us to isolate and identify a novel rat OBP (*13*) and an aphrodisiac lipocalin from hamster vaginal discharges (*40*). Human samples were taken at different levels of the nasal cavity (inferior turbinate, septum, olfactory cleft) of several patients under endoscope. We observed a few differences in the RPLC profiles of mucus sampled at a given level from one subject to another, and even from one nostril of a single

patient to another. Nevertheless, the set of chromatographic peaks over 43% acetonitrile was observed to be specific of the olfactory cleft mucus. Figure 1 presents the comparison of typical RPLC profiles obtained from the same patient to emphasize differences between mucus sampled at different places. During chromatography, fractions were collected and analyzed by MALDI-TOF mass spectrometry. The chromatographic profile of the olfactory cleft mucus (Figure 1A) is clearly different from samples originating from the inferior turbinate (Figure 1B) and the septum (Figure 1C), particularly when CH_3CN percentage was above 43%. For lower CH_3CN concentrations, eluting molecules were mainly peptides and protein fragments smaller than 10 000 Da, as shown by mass spectrometry. For the olfactory cleft sample, identifications of major fractions (F1 to F8) were performed by Edman sequencing and searches in databases. In fractions F1, F2, and F5, we found α-hemoglobin (Swiss-Prot # P01922) beginning at the N-terminus, while in fraction F2, β-hemoglobin (Swiss-Prot # P02023) was identified as a fragment beginning at position 33, and in fraction F4 the same protein was found beginning at position 42. The expected mass of α-hemoglobin is 15 126 Da, it was found with a mass of 15 108 and 15 107 Da in F7 and F8, respectively, while that of β-hemoglobin, expected to be 15 867 Da was measured to be 15 864 and 15 865 Da in the same fractions, respectively. Antileukoproteinase (Swiss-Prot # P03973), beginning at position 1, was observed in fraction F1 with a mass of 11 705 Da (expected 11 710) and lysozyme (Swiss-Prot # P00695) in fractions F3 and F4, beginning at position 1 with a mass of 14 690 Da (expected 14 693). None of the identified proteins at a CH_3CN concentration under 43% in any mucus sample could be assigned to an OBP, even to a lipocalin. Whereas no peak was found in both inferior turbinate and septum samples above this percentage, several proteins were observed specifically in the olfactory cleft mucus. Above 43% CH_3CN, three peaks (fractions F6, F7 and F8) were shown to contain human serum albumin (Swiss-Prot # P02768), α- and β-hemoglobin chains and fragments. Interestingly, in fraction F8 eluting at around 49% CH_3CN, we also found two N-terminal sequences (EDITGTWYVK and WYVKAMVVDK), absent from all other fractions. They have been unambiguously identified in the Genpept library as fragments of human putative OBPs (Genpept # AJ251021, 22, 24, 25, 26, 27, and 29) corresponding to N-terminal ends beginning at residues 8 and 14, respectively (Figure 2). Two sets of molar masses were obtained, one ranging from 14 695 to 14 993 Da and the other from 14 078 to 14 377 Da. The first set corresponds to proteins beginning at E8 and ending at either residues H134, K135, G136, and L137, while the second set corresponds to proteins beginning at W14 with the same heterogeneous C-termini. In addition to the 2 N-terminal excisions of 7 and 13 residues, hOBP molecules underwent a C-terminal cleavage of 20 ± 2 residues. Various hOBP fragments were observed in the olfactory cleft mucus of different patients. Among these fragments, we found a N-terminal peptide of 10 764.3 Da beginning with the sequence LSFTLEEEDI. It corresponds to L1−D94 (Figure 2), starting at the predicted N-terminus of the mature protein deduced from the nucleotide sequence (*34*), cleaved before the seventh β-strand. In summary, putative OBP derivatives were observed solely in the mucus of the olfactory cleft. As these proteins were not

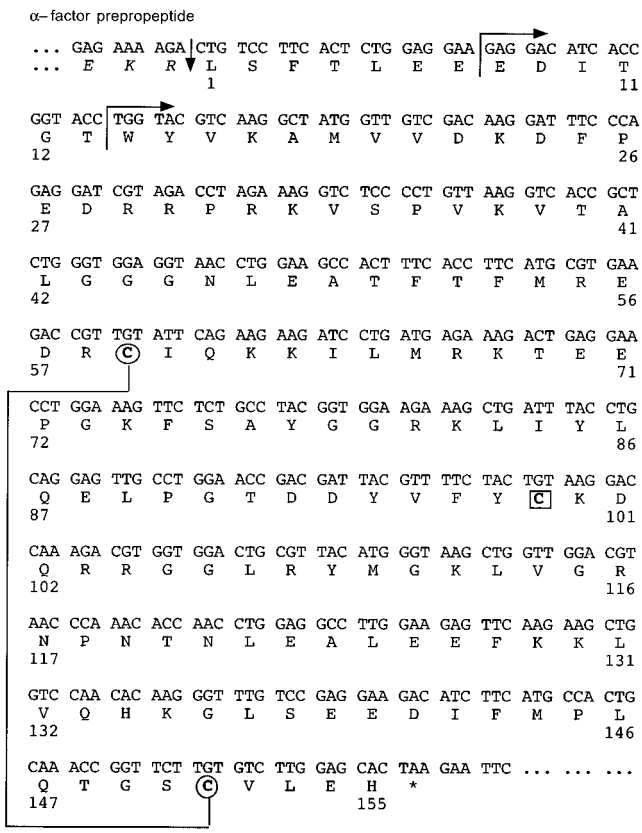

FIGURE 2: Synthetic cDNA sequence of $hOBP_{IIa\alpha}$. Nucleotide sequence of the synthesized DNA encoding $hOBP_{IIa\alpha}$ with its deduced amino acid sequence. Amino acids from the *Saccharomyces cerevisiae* α-factor propeptide signal are in italics (only a small part of this sequence is shown). The asterisk marks the stop codon. Amino acids are numbered from the first L of the predicted mature sequence. The vertical arrow indicates the cleavage site of the recombinant protein. Arrows at positions 1, 8, and 14 show the N-terminal ends observed in the proteins of the olfactory cleft mucus. The free cysteine is boxed and the disulfide bond is indicated by a line connecting the circled half-cystines.

detected in the mucus sampled at the surface of either the inferior turbinate or the septum, their presence could indeed be limited to the uppermost region of the nasal cavity where odorant molecules are detected by olfactory receptor neurons.

$hOBP_{IIa\alpha}$ Heterologous Expression and Purification. $hOBP_{IIa\alpha}$ was expressed using the methylotrophic yeast *Pichia pastoris*. For this purpose, a gene encoding $hOBP_{IIa\alpha}$, with codons optimized for expression in *Saccharomyces cerevisiae*, was synthesized (Figure 2). The protein was secreted using the yeast prepropeptide signal from the *S. cerevisiae* α mating-factor peptide. Approximately 500 transformants of the GS115 strain were obtained by electroporation, and 100 transformants were screened for their resistance to G418. Forty multiple copy transformants resisting to 2 mg/mL G418 corresponding to Mut^s phenotype were screened by SDS−PAGE for their capability to secrete high amounts of $hOBP_{IIa\alpha}$. One clone was selected for its high level of recombinant protein secretion. Culture supernatants taken at various time intervals showed that the protein regularly accumulated for 3 days (not shown), while no other protein was detectable. Proteolysis was reduced by adding 2% tryptone and 5 mM EDTA in the induction culture medium, which was adjusted to pH 8.0. Approximately 10 mg of purified protein were obtained per filtrate liter over an

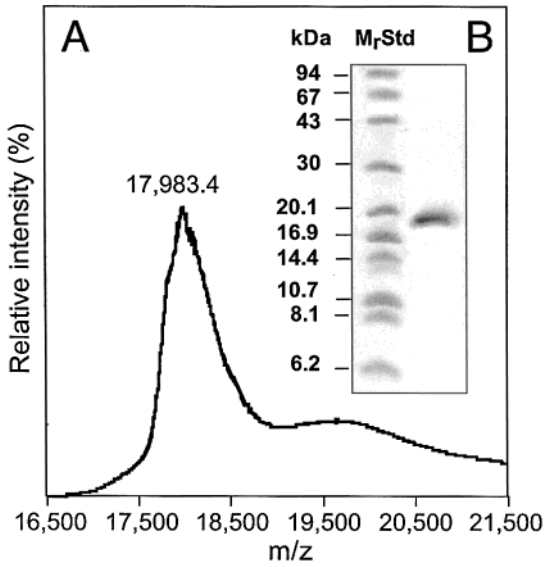

FIGURE 3: Electrophoretic and mass spectrometry analysis of the recombinant $hOBP_{IIa\alpha}$. (A) MALDI-TOF mass spectrum of recombinant $hOBP_{IIa\alpha}$ secreted by *Pichia pastoris*. (B) SDS−PAGE of purified $hOBP_{IIa\alpha}$. The lane marked M_rSTD shows molecular weight standards (Pharmacia LMW and PMW kits).

expression period of 3 days. After centrifugation of the sample, the yeast culture filtrate was dialyzed, precipitated under acidic conditions, and submitted to ion-exchange HPLC to retain contaminants on the column. When necessary, a further purification step was conducted through gel filtration for desalting.

Recombinant Protein Characterization. SDS−PAGE analysis of the purified protein shown in Figure 3B reveals absence of contaminants, as ascertained by sequencing which showed a single sequence with LSFT at the N-terminus. MALDI-TOF mass spectrometry (Figure 3A) showed a major broad protein peak with shoulders exhibiting a mean molecular mass of 17 983.4 Da. The theoretical mass deduced from the cDNA sequence beginning with LSFT and one formed disulfide bridge is 17 828.6 Da. The mean mass excess of 154.8 Da could not be assigned to any obvious posttranslational modification, which suggested variable alkylation of the single free cysteine.

The disulfide bridge pairing of $hOBP_{IIa\alpha}$ was investigated by CNBr chemical cleavage of unreduced recombinant protein and peptide mapping of the digest. Peptides resulting from CNBr digestion were separated and analyzed by both MALDI-TOF and microsequencing. As shown in Figure 4, the first peptide was obtained as a doublet peak eluting at approximately 15% CH_3CN corresponding to peptides with homoserine lactone and homoserine derivative, respectively. Its monoisotopic *m*/*z* of 2665.36 corresponded to the sum of the masses of the two peptides P145−H155 (C-terminus) and R55−M66 linked by a disulfide bond (calculated *m*/*z* 2665.39). In addition, this peak was submitted to Edman sequencing, showing the sequences of these two peptides in equimolar amounts (approximately 20 pmol) for 12 cycles, which confirmed the disulfide bond between C59 and C151. In the second peak (∼21.5% CH_3CN), sequencing showed two peptides, V20−M54 with a *m*/*z* of 3829.25, in good agreement with the calculated value (3829.04), and R67−M110 with a 154.5 average mass excess. In the third peak (∼24.5% CH_3CN), sequencing exhibited two peptides,

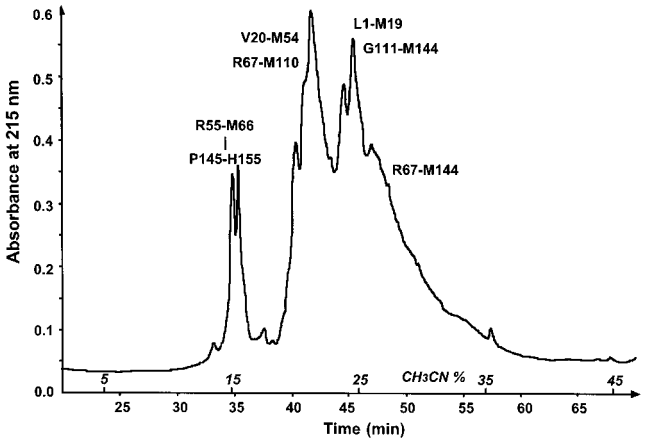

FIGURE 4: Mapping of CNBr $hOBP_{IIa\alpha}$ peptides. Reversed phase liquid chromatography of peptides resulting from CNBr cleavage of unreduced $hOBP_{IIa\alpha}$. The sequences deduced from MALDI-TOF analysis and N-terminal sequencing are indicated by residues positions over the analyzed peaks.

Table 1: Identification of Reduced and Alkyled $hOBP_{IIa\alpha}$ Tryptic Peptides by MALDI-TOF Mass Spectrometry

peptide identification	theoretical mass $(M + H)^+$ (alkylated peptides)	measured mass $(M + H)^+$
L1-K17	2031.00	2030.89
A18-R29	1421.67	1421.67
R30−K38	1066.68	1066.48
V39−R58	2185.07	2185.06
C59−K62	548.29	not found
I64−K68	660.42	660.40
K68−R81	1526.76	1526.79
T69-R81	1398.66	1398.69
L83-K100	2237.08	2237.06
L83-R103	2636.27	2636.32
R104−R108	558.35	558.33
Y109−K129	2423.24	2423.15
N117−K135	2252.20	2252.20
G136-H155	2262.04	2261.96

G111−M144 (*m*/*z* 3836.49 in good agreement with the calculated value, 3836.03) and L1−M19 with a *m*/*z* of 2201.07 with a *m*/*z* excess of 16.0. Sequencing revealed the absence of tryptophan PTH at position 14. Instead, we observed a PTH of a tryptophan derivative, which eluted before the proline PTH. Oxidation of tryptophan was then suspected to occur during the CNBr cleavage reaction, since it was not observed in the tryptic digest (see below). In the fourth peak (∼27% CH_3CN), the peptide R67−M144 was identified by sequencing from R67 to G111. It exhibited a broad mass peak centered at average *m*/*z* 9179.2, with a *m*/*z* excess of 151.9 with regard to the calculated *m*/*z*. No PTH derivative could be observed at the position corresponding to C99, which showed that only C99 was modified.

To confirm that alkylation of the free cysteine was the only alteration of recombinant $hOBP_{IIa\alpha}$, reduced and alkylated protein was submitted to trypsinolysis, and the resulting peptides were analyzed by MALDI-TOF mass spectrometry (Table 1). Except peptide C59−K62, all the expected tryptic peptides were observed and identified. The N-terminal peptide L1−K17 exhibited a *m*/*z* of 2030.89 in good agreement with the calculated monoisotopic *m*/*z*, showing that W14 was not oxidized. In addition, it is worth noticing that, after reduction and alkylation of the sample, the sizes

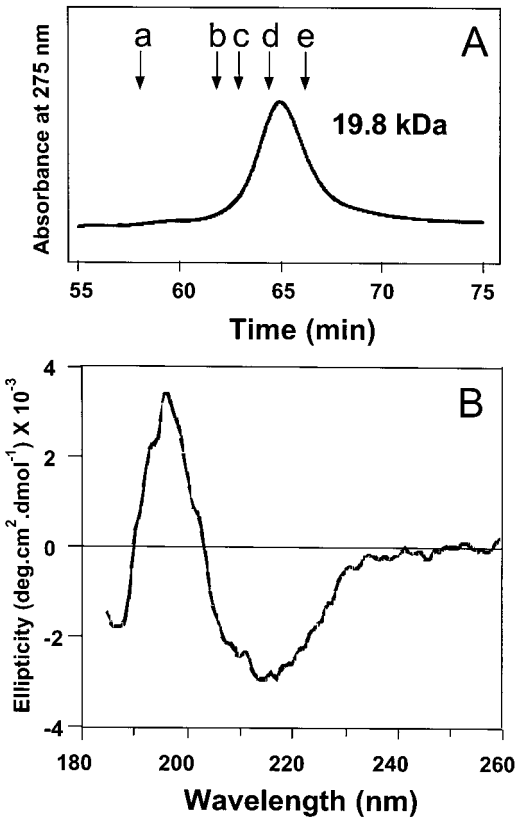

FIGURE 5: Secondary and quaternary structure of the recombinant $hOBP_{IIa\alpha}$. (A) Exclusion-diffusion chromatography on Superose 12. The elution positions of the molecular weight standards are indicated by arrows: (a) chicken egg ovalbumin (43 kDa); (b) dimeric bovine β-lactoglobulin (36 kDa); (c) bovine carbonic anhydrase (30 kDa); (d) soybean trypsin inhibitor (21.5 kDa); (e) bovine ribonuclease A (13.7 kDa). (B) Secondary structure determination by circular dichroism spectroscopy. Protein concentration was approximately 0.5 mg/mL and path length 0.01 cm.

of the peptides comprising C99 (L83−K100 and L83−R103) were found to be monodisperse with *m*/*z* corresponding to alkylated forms. This demonstrates that the mass excess of the recombinant protein only originated in variable alkylation of C99.

Calibrated exclusion-diffusion chromatography of purified $hOBP_{IIa\alpha}$ at 0.5 mg/mL gave an apparent molar mass of 19.8 kDa, which is close to the value obtained from mass spectrometry, demonstrating that the recombinant protein exists as a monomer at neutral pH (Figure 5A). Figure 5B shows the CD spectrum of recombinant $hOBP_{IIa\alpha}$ in phosphate buffer. The shape of the spectrum, i.e., the maximum at 195 nm and the minimum at 217 nm, clearly showed the presence of a high percentage of β-sheet in the protein (~60%) and few or no α-helix. The recombinant protein appeared therefore quite amenable to odorant-binding studies, since it was chemically homogeneous and properly conformed, with its disulfide bridge formed and a secondary structure as expected for a lipocalin.

Fluorescent Binding Assay. We first tested the capability of $hOBP_{IIa\alpha}$ to bind fatty acids, since it exhibits a greater sequence homology with rat OBP-2 known to preferentially interact with alkyl molecules (*28*). Automated modeling of the 3D structure of $hOBP_{IIa\alpha}$ showed that the spatially conserved single tryptophan residue (W14) was inside the binding pocket, separating the crevace from the outside (Figure 6). We therefore assayed tryptophan fluorescence as an intrinsic probe, known to be quenched upon ligand binding in several members of the lipocalin superfamily (*44*−*46*). Among halogenated compounds, which are known to strongly quench tryptophanyl residues (*47*, *48*), we tried two bromo-substituted fatty acids, BrC12-Ac and BrC15-Ac, but without success.

We then tested the ability of $hOBP_{IIa\alpha}$ to bind several extrinsic fluorescent probes, beginning with fatty acid analogues, DAUDA, DACA, and ASA (*49*, *50*). When excited at 345 nm, DAUDA presented a weak fluorescence emission with a maximum at 545 nm in aqueous medium (Figure 7B). In presence of $hOBP_{IIa\alpha}$, the maximum underwent an hypsochrome shift toward 490 nm with a 10-fold quantum yield increase. Titration of $hOBP_{IIa\alpha}$ with DAUDA was saturable ($K_d = 1.5 \pm 1.3$ μM) with one binding site per monomer (Figure 7D). Other fluorescent fatty acids, DACA and ASA, were found to bind $hOBP_{IIa\alpha}$ with apparent dissociation constants of 8.1 ± 4.9 and 0.97 ± 1.0 μM, respectively (data not shown). Their emission maxima were blue shifted to 475 and 425 nm, respectively.

In addition, we assayed fluorescent polycyclic probes known to bind several OBPs, 1-AMA, and 1,8-ANS (*13*, *16*, *23*, *28*, *51*). The fluorescence spectrum of 1-AMA was not found to be altered when mixed with $hOBP_{IIa\alpha}$ (data not shown), opposite to 1,8-ANS whose maximum emission was shifted to 468 nm with a K_d of 12 μM. Nevertheless, 1,8-ANS was found to be unable to be competitively displaced by any of the ligands employed. Moreover, by reference to the mouse major urinary proteins, known to bind odorants (*52*), we used NPN, which proved to be a fluorescent ligand for $hOBP_{IIa\alpha}$. The binding of NPN induced a 40-fold increase of fluorescence intensity and a blue shift of the maximum emission wavelength toward 400 nm, when excited at 337 nm (Figure 7A). The saturation curve of NPN onto $hOBP_{IIa\alpha}$ (Figure 7C) exhibited an apparent dissociation constant of 3.3 ± 1.9 μM and a single binding site per monomer.

Ligand Competitive Assays using Fluorescent Probes. Diverse odorant compounds, which represent several classes of chemical structures, and odors were used in competitive fluorescence binding assays using both NPN and DAUDA as probes. We verified that the reaction equilibrium was reached before data collection. We also tested MeOH, which was used to dissolve ligands and probes, for its capacity to compete with fluorophores. As already reported for rat OBP-1F (*13*), no effect was observed with this solvent. Results were comparable whatever the probe used, as shown by the mean deviation between K_{diss} measured with either NPN or DAUDA found to be lesser than 30%, variations typical for such measurements. It is noteworthy that, in each chemical series, K_{diss} varied in parallel, whatever the probe used. Seven odorants (IBMP, α-pinene, eugenol, γ-decalactone, citralva, β-ionone, and vanillin) were shown to have different abilities to displace the fluorescent probes. As shown in Figure 7E,F, the fluorescence intensity of the $hOBP_{IIa\alpha}$ probe complexes were severely reduced with vanillin and, to a lesser extent, with citralva, α-pinene, and IBMP, while the effects of eugenol, γ-decalactone, and β-ionone could be considered as negligible. The calculated apparent dissociation constants (K_{diss}), deduced from the half-maximal values (IC_{50}), were very high for these latter compounds, while citralva, α-pinene, and IBMP exhibited intermediate affinity constants (Figure

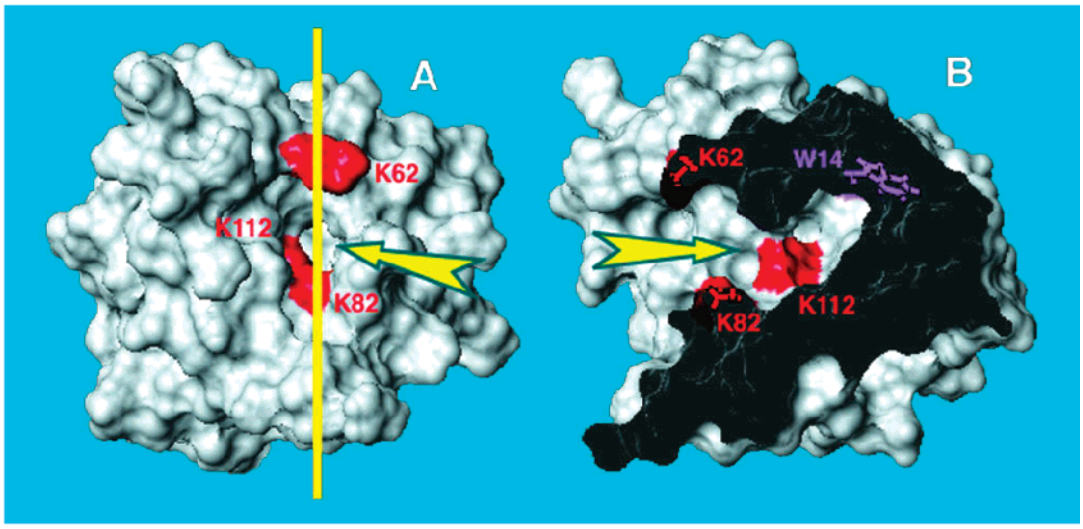

FIGURE 6: Views of molecular surface of the predicted tertiary structure of $hOBP_{IIa\alpha}$. Automated alignment and modeling were performed with the major horse allergen (PDB accession number 1EW3A). (A) Front view of the protein with opening of the binding pocket indicated by an arrow. (B) Rotation of 90° showing a vertical section of the model through the binding pocket, as indicated by a yellow line in panel A. In the binding pocket, lysine side chains and surfaces are colored in red, tryptophan in violet.

8). In any case, we noticed that the ligand affinity for $hOBP_{IIa\alpha}$ was correlated to the amount of fluorescence reduction, which reveals the displacement (*d*) of probes by odorants.

To know the molecular parameters guiding the affinity of odorants for $hOBP_{IIa\alpha}$, we first investigated the influence of their size, using fatty acids as models and then tried to elucidate the potential role of functional groups. The fatty acid chain length was correlated to affinity, since displacement of probes was observed to regularly increase from octanoic acid ($K_{diss} \sim 2$ μM) to palmitic acid ($K_{diss} = 0.3$ μM), which was found to be one of the best tested ligands. In this series, we included the two brominated fatty acids, previously assayed for tryptophan fluorescence quenching. They were found to efficiently compete with both probes, but conspicuously less than non-brominated fatty acids of the same size. To investigate the influence of functional groups, octane derivatives were tested. As reported in Figure 8, the two aldehyde derivatives of this series proved to be potent competitors ($K_{diss} < 2$ μM), far more efficient than 1-octanol and 2-octanone, but less than octane ($K_{diss} \sim 1.5$ μM). The nitrile functional group (citralva) also displayed enhancer effects, but to a lesser extent. Comparison of 10-carbon aliphatic molecules supports the assumption that aldehyde derivatives are more efficient than others. In addition, 10-carbon aliphatic molecules showed a better affinity for $hOBP_{IIa\alpha}$ than the equivalent 8-carbon molecules. The influence of aldehyde derivative size was then studied by comparison with that of fatty acids. Like acids, aliphatic aldehydes were the more efficient as long aldehydes, but with a maximum reached at an 11-carbon length. Up to this length, their ability to displace both DAUDA and NPN was equivalent to that of fatty acids with 4 to 5 more carbons, indicating that the aldehyde group increases the odorant affinity, which is chiefly caused by hydrophobic interactions. We also observed that the affinity of all the tested benzenic and heterocyclic aldehydes was better than that of fatty acids with a same number of carbons.

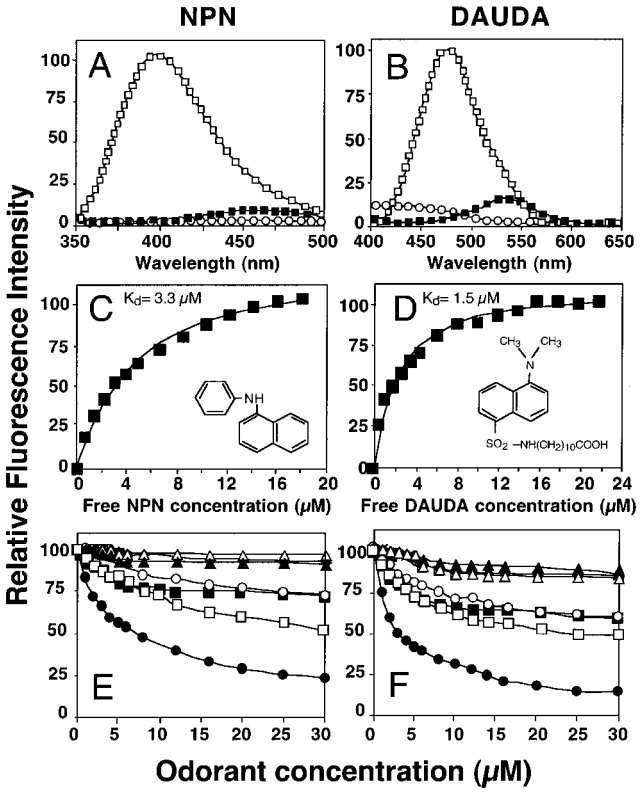

FIGURE 7: NPN and DAUDA fluorescence binding assay. Fluorescence emission spectra recorded at 25 °C of 4 μM NPN (A) and DAUDA (B) in the presence of 2 μM recombinant $hOBP_{IIa\alpha}$ (open squares); solid squares indicate the fluorescence of probes alone (4 μM) and open circles indicate protein solution alone (2 μM); excitation wavelengths were 337 and 345 nm for NPN and DAUDA, respectively. Titration curves of NPN (C) and DAUDA (D); solid squares show experimental data, while solid lines are the computed binding curves; excitation wavelengths and protein concentrations were as in panels A and B; emission wavelengths were 400 and 490 nm, for NPN and DAUDA, respectively; probes formulas are inserted. Competitive binding assays of NPN (E) and DAUDA (F) with several odorants: *2*-isobutyl-*3*-methoxypyrazine (■), *β*-ionone (◆), α-pinene (○), citralva (□), *γ*-decalactone (△), eugenol (▲), and vanillin (●); fluorescence of probe−protein complexes were assigned to 100% in the absence of competitor; experimental conditions were as above.

Ligand	Structure	NPN d %	NPN IC_{50} µM	NPN K_{diss} µM	DAUDA d %	DAUDA IC_{50} µM	DAUDA K_{diss} µM
Diverse odorants							
2-methoxy-*4*-(*2*-propenyl) phenol (eugenol)	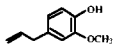	9	>20	>8	13	>30	>10
gamma-*n*-hexyl-gamma-butyro lactone (γ-decalactone)	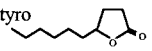	4	>30	>12	18	>20	>7
4-(*2,6,6*-trimethyl-*1*-cyclohexen-*1*-yl)-*3*-buten-*2*-one (β-ionone)		7	>20	>8	17	>20	>7
(*1S,5S*)-*2,6,6*-trimethyl-bicyclo-[*3.1.1*]-*2*-heptene (α-pinene)		25	7.5	3.0	40	5.0	1.7
3,7-dimethyl-*2,6*-octadiene-*1*-nitrile (citralva™)	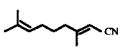	48	8.0	3.2	50	4.6	1.5
2-isobutyl-*3*-methoxypyrazine (IBMP)		25	2.8	1.1	36	2.8	0.9
4-hydroxy-*3*-methoxy-benzaldehyde (vanillin)		81	3.5	1.4	85	2.0	0.7
Fatty acids							
octanoic (caprylic) acid		25	6.0	2.4	46	5.0	1.7
decanoic (capric) acid	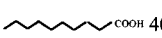	40	5.2	2.1	50	4.5	1.5
dodecanoic (lauric) acid		65	3.0	1.2	76	3.2	1.1
tetradecanoic (myristic) acid		65	1.3	0.5	72	2.0	0.7
hexadecanoic (palmitic) acid		65	0.9	0.4	70	1.0	0.3
12-bromododecanoic acid (BrC12-Ac)	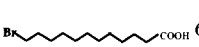	60	3.2	1.3	33	5.0	1.7
15-bromopentadecanoic acid (BrC15-Ac)	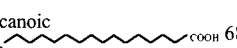	68	1.4	0.6	68	2.6	0.9

Ligand	Structure	NPN d %	NPN IC_{50} µM	NPN K_{diss} µM	DAUDA d %	DAUDA IC_{50} µM	DAUDA K_{diss} µM
8-carbon odorants							
1-octanol	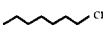	23	10	4.0	30	10	3.3
2-octanone	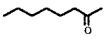	25	6.0	2.4	20	8.0	2.7
2-octene		44	7.0	2.8	38	5.0	1.7
trans 2-octenal		61	5.2	2.1	42	6.0	2.0
n-octane		54	4.0	1.6	40	4.0	1.3
n-octanal		46	2.8	1.1	50	2.5	0.8
10-carbon odorants							
1-decanol		46	6.0	2.4	60	7.0	2.3
(±)-*3,7*-dimethyl-*6*-octen-*1*-ol (citronellol)	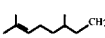	30	5.0	2.0	20	5.0	1.7
3,7-dimethyl octanal	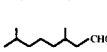	70	1.8	0.7	55	6.0	2.0
2-trans-3,7-dimethyl-*2,6*-octadien-*1*-ol (geraniol)		30	3.0	1.2	42	3.8	1.3
(±)-*3,7*-dimethyl-*6*-octen-*1*-al (citronellal)		62	2.1	0.8	73	2.5	0.8
Aldehydes							
n-hexanal		31	8.0	3.2	45	9.0	3.0
n-heptanal		58	3.8	1.5	52	5.0	1.7
n-nonanal		65	2.2	0.9	70	1.8	0.6
n-decanal	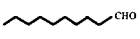	74	1.4	0.6	77	1.5	0.5
n-undecanal		70	1.0	0.4	80	1.0	0.3
n-dodecanal		66	1.2	0.5	86	1.5	0.5
benzaldehyde		45	5.0	2.0	36	4.0	1.3
α-methyl-*3,4*-(methylenedioxy)-hydro cinnamaldehyde (helional™)	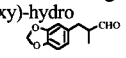	55	4.0	1.6	70	3.0	1.0
2-methyl-*3*-(*4-tert*-butylphenyl) propanal (lilial™)		60	1.5	0.6	75	1.2	0.4

FIGURE 8: Affinity of ligands for $hOBP_{IIa\alpha}$. Data are gathered according to comparative experiments and classified following increasing affinity among each group. Ligands are named both after their chemical names and common names (between brackets). Competitions were performed with both NPN and DAUDA as fluorophores; *d*, maximal percentage of displacement reached at high ligand concentration; IC_{50}, ligand concentration provoking a decay of fluorescence of half-maximal intensity; K_{diss}, apparent dissociation constant obtained by $K_{diss} = [IC_{50}]/(1 + [L]/K_d)$ with [L] for the free probe concentration and K_d the measured dissociation constants of OBP−probe complexes. Experimental conditions were those of Figure 7.

DISCUSSION

Biochemical investigation of different levels of the nasal cavity of human patients revealed truncated protein isoforms homologous to recently described genes coding for putative OBPs. Observation of peptides was emphasized by RPLC, a method that is particularly suited for peptide separation, whereas 2-dimensionnal electrophoresis cannot reveal low molecular weight molecules. OBP truncation was mainly limited to exoproteolysis, since, in addition to the two N-terminal excisions of 7 and 13 residues, the molecule undergoes a C-terminal cleavage of 20 ± 2 residues. We nevertheless observed endoproteolysis to occur after D94 in an external loop between β-strands 6 and 7, without N-terminal proteolysis. Such cleavages were recently shown by 2-dimensional gel electrophoresis to occur in human nasal lavage fluid, in which albumin and tear lipocalin were observed as many short peptides or truncated fragments (*53*). OBP isoforms were observed to be solely secreted in the olfactory cleft mucus where the olfactory epithelium is situated. Human olfactory epithelium, containing sensory neurons, is situated on the cribriform plate and extents inferiorly for a short distance on the septum, the superior turbinate, and, possibly, the upper part of the middle turbinate (*54*). Human olfactory epithelium is similar in organization and cell morphology to that of most vertebrate species, with numerous secretory Bowman's glands in the lamina propria. It covers a surface of about 100−400 mm^2 in the uppermost part of the nasal cavity, named the olfactory cleft (Figure 1). A recent study demonstrated, by biopsy and electrophysiological recordings, that this anterior part contains olfactory neurons which generate odor-induced electrical responses in a majority of subjects (*55*). Presence of $hOBP_{IIa\alpha}$ only in the olfactory cleft is partly in disagreement with localization of mRNAs, which were detected in acinar cells from the middle meatus and turbinates, but not searched in the olfactory cleft (*34*). The secretion site of this protein is however in accordance with location of Bowman's glands in the human sensory olfactory epithelium (*54*). These glands have been shown in other species to contribute to the secretion of OBPs (*56*). Previous trials to find OBPs in the human nasal cavity (*29*−*33*) have failed, probably because these approaches were based on analysis of washings of the whole nasal cavity in which proteolysis could occur (*53*). The small area of the olfactory cleft, which can be estimated

to less than 10% of the total area of the nasal cavity in humans, and its inaccessible location (*54*) make difficult the sampling of the olfactory cleft mucus. In contrast to other authors, we did not observe tear lipocalin, which is secreted both in lachrymal and seromucous glands of the human nasal mucosa (*29*, *30*). Abnormal retention on RPLC column or proteolysis (*53*) may explain such an absence.

The specific location of human OBPs in the olfactory cleft suggests its role as an odorant carrier. To test their ability to bind odorants, we expressed a hOBP gene variant, which was shown to be transcribed in the nasal structures (*34*). Using the *Pichia pastoris* system, we obtained $hOBP_{IIa\alpha}$ as a well-conformed lipocalin with its single typical disulfide bond properly formed and a single expected N-terminus. A ligand binding study was then performed, since no artifactual alteration of the molecule occurred, with the exception of variable alkylation of the free sulfhydryl group located at the sill of the binding pocket, as predicted by molecular modeling (not shown).

We found that $hOBP_{IIa\alpha}$ exists as a monomer at neutral pH like several OBPs (*7*, *23*), while some others are known as dimers, such as rat OBP-2 (*28*). Another difference between $hOBP_{IIa\alpha}$ and this rat OBP lies in the isoelectric point. $hOBP_{IIa\alpha}$ is neutral (calculated pI 7.8, measured pI 6.5), opposite to rat OBP-2, which is clearly basic (calculated pI 9.0), while the typical nature of OBPs is acidic. Lipocalins exhibit a common disulfide bond pattern, revealing one or two bridges. One of them, immobilizing the C-terminal structure formed by an α-helix and an antiparallel β-strand, appears to be more important for the global structure of the molecule than the other disulfide bond when present (*3*). Although comprising four cysteines, porcine OBP-3 has been reported to exhibit only this single disulfide bond (*16*), observed in $hOBP_{IIa\alpha}$ (C59−C151), which exhibited a free cysteine (C99). In the mouse major urinary protein, this bridge was also observed (C68−C161), whereas C142 remained free (*57*). Although not yet determined, the occurrence of only three cysteines in the rat OBP-2 suggests a similar arrangement. It is worth comparing $hOBP_{IIa\alpha}$ with the human tear lipocalin (identical to the Von Ebner's Gland protein), which belongs to the same gene cluster and is expressed in the nasal sphere (*58*). $hOBP_{IIa\alpha}$ and the human tear lipocalin exhibit 45.2% sequence identity with a similar cystein pattern. The main difference is located at the N-terminus, which is known to be involved in the protease inhibitor activity of the tear lipocalin. The comparison of the predicted 3D models of $hOBP_{IIa\alpha}$ and human tear lipocalin (not shown) reveals an important difference, which involves the β-barrel forming the calix. Whereas the lipocalin supersecondary structure was found to be canonical in the $hOBP_{IIa\alpha}$ model, the first and sixth β-strands of the tear lipocalin were in aperiodic structure. Moreover, an aperiodic structure corresponding to the first lipocalin β-strand was observed to obstruct the putative binding pocket. In addition, the residues homologous to those which are tightly assembled to make the $hOBP_{IIa\alpha}$ binding pocket are scattered in the predicted tear lipocalin model. When comparing $hOBP_{IIa\alpha}$ with rat OBP-2, we observed that 45% of the residues forming the binding pocket are identical, which is close to the equivalent comparison between $hOBP_{IIa\alpha}$ and the tear lipocalin (48%). Nevertheless, opposite to the tear lipocalin, the rat OBP-2 3D model (not shown) revealed that these residues formed a typical lipocalin binding pocket slightly larger than that of $hOBP_{IIa\alpha}$. These structural differences support the functional divergence between OBPs and tear lipocalin.

The binding site of $hOBP_{IIa\alpha}$ certainly lies in the hydrophobic pocket within the β-barrel, as attested by the spectral properties of probe fluorescence emission. When bound to hOBP, maximal emission wavelengths of dansyl probes decreased while quantum yields increased, revealing a deep burying into an apolar environment. DACA, which exhibited a maximum at 475 nm, is likely taken into the binding site in its entirety, as already reported for uterocalin, a lipocalin with fatty acid and retinol binding properties (*59*). It would be more deeply buried than DAUDA (maximal emission wavelength 490 nm), which is a larger molecule. With regard to NPN, an aromatic probe, the hypsochrome shift indicated a very apolar environment (*60*), whereas ASA blue shift would essentially reflect steric hindrance of this anthroyloxy derivative within the hydrophobic cavity (*61*). In contrast to rat OBP-2 (*28*), we noticed that 1,8-ANS was not displaced by odorants, as already observed for bis-ANS (1,1′-bis(4-anilino-5-naphthalene)-sulfonic acid) with rat OBP-3 (*23*). The blue shift of the emission spectrum of 1,8-ANS when bound to $hOBP_{IIa\alpha}$ was limited, suggesting binding onto the surface of the protein, in accordance with the absence of competition with ligands. It is therefore likely that odorants and fatty acids enter the β-barrel pocket, with their hydrophobic moiety inside, as already reported for interactions of 1-AMA with bovine OBP (*42*) and diverse odorants with porcine OBP (*62*). The lower affinity of the brominated fatty acids, compared to unsubstituted ones, can be explained either by steric hindrance caused by the Br atom or by electrostatic interactions with lysyl residues located at the edge of the pocket (Figure 6). In any case, this atom would prevent the molecule to deeply enter the pocket, as attested by the absence of quenching of the intrinsic fluorescence of W14, which is situated at the very bottom of the binding pocket. Regarding the affinity enhancement observed for aldehyde compounds compared to the corresponding fatty acids, formation of hydrogen bonds between the aldehyde group and the amine function of a lysyl residue at the rim of the calix could stabilize the docking of the odorants, as suggested for K70 in β-lactoglobulin−chromophore interaction (*63*). The 3D model of $hOBP_{IIa\alpha}$ suggests that K82 and 112, and less plausibly K62, are candidates for playing such a role. It is tempting to hypothesize that, when aliphatic aldehyde molecules comprise more than 11 carbons, such aldehyde−lysine interactions are hampered by the size of the aliphatic chain, resulting in reduction of affinity. The observation that fatty acids, opposite to aldehyde derivatives, do not exhibit a decrease in affinity when their size increases supports this hypothesis. In addition, it is worth noticing that rat OBP-2 does not preferentially bind aldehyde derivatives (*27*) and that the predicted structure of its binding pocket exhibits only one lysine (K112), instead of three for $hOBP_{IIa\alpha}$. This suggests that at least one of the two other lysines, probably K82, is involved in aldehyde binding. The benzenic and heterocyclic aldehydes, especially lilial, which bind very efficiently to $hOBP_{IIa\alpha}$, need further investigation to understand the binding mode before reaching a similar conclusion. Nevertheless, hydrophobic interactions are likely the main forces driving the binding of odorants onto $hOBP_{IIa\alpha}$, since

hydrocarbons such as α-pinene and octane exhibit high affinity.

Although NPN, an aromatic molecule, and DAUDA, a fatty acid with an aromatic fluorophore, are quite different, we observed a common behavior upon displacement with various ligands. This suggests that both probes bind the same site, which is very likely the binding pocket, as observed for bovine OBP with 1-AMA probe (*42*). DACA and ASA were only partially studied, but allowed similar conclusions. As noticed for competitors, the affinity of probes derivated from fatty acids increased with the length of the aliphatic chain, from DAUDA (chain of 11 carbons) to ASA (18 carbons). The affinity of all the tested probes for $hOBP_{IIa\alpha}$, in the micromolar range, were quite analogous to those observed with other probes and various OBPs (*13*, *16*, *23*, *28*, *51*, *64*). Regarding 1-AMA, porcine OBP-2 (*16*) was also reported not to bind this probe. Lastly, the dissociation constant observed for NPN was close to those measured with other tested probes (DAUDA, DACA, and ASA), but 50-fold higher than those described for MUP variants (50 to 60 nM). However, NPN binds MUP variants some 20-fold more tightly than the natural ligand 2-*sec*-butyl-4,5-dihydrothiazole (*52*).

We demonstrated that $hOBP_{IIa\alpha}$ was indeed able to bind diverse odorants with a dissociation constant in the micromolar range, as all known vertebrate OBPs. When comparing odorant affinity, $hOBP_{IIa\alpha}$ can be characterized by its low affinity for some very potent odorants, such as eugenol ($K_{diss} > 10\ \mu M$), and a high affinity for aldehydes, such as undecanal ($K_{diss} \sim 0.3\ \mu M$), lilial, the odor of the lily of the valley ($K_{diss} \sim 0.5\ \mu M$), and vanillin ($K_{diss} \sim 1\ \mu M$), and also large fatty acids ($K_{diss} \sim 0.3\ \mu M$). Comparison of the specificity of $hOBP_{IIa\alpha}$ to other vertebrate OBPs leads us to point out some similarities. Although not very strict, $hOBP_{IIa\alpha}$ specificity can contribute to odor discrimination, as suggested for rat OBP-1, 2, and 3, which were shown to be complementary in odorant binding (*23*, *28*, *64*). Opposite to other known OBPs, rat OBP-2, whose sequence is closest to that of $hOBP_{IIa\alpha}$, binds fatty acids preferentially to aldehydes (*28*), so we expected to find a similar specificity. The apparent dissociation constants we observed are indeed very close to those reported for the binding of fatty acids on rat OBP-2; nevertheless, $hOBP_{IIa\alpha}$ binds more efficiently the larger chains. As also observed with rat OBP-2, we noticed the binding of citralva and lilial, but with a better affinity. In contrast to rat OBP-2, we observed that IBMP and benzaldehyde bind $hOBP_{IIa\alpha}$, suggesting that differences in the structure of the binding pockets result in variations in specificity.

The structural homology of $hOBP_{IIa\alpha}$ with other vertebrate OBPs and its location in the olfactory cleft mucus support its role in olfaction. Furthermore, hOBP clearly binds many odorants. In addition, it structurally differs from the tear lipocalin, another lipocalin strongly expressed in the nasal cavity (*29*, *30*), which has both a proteinase inhibitor role and an endonucleasic activity, likely involved in nonimmunological defense against pathological organisms (*58*, *65*). The olfactory function of $hOBP_{IIa\alpha}$ is therefore very plausible. Its distribution in other tissues has nevertheless still to be studied at the protein level, since mRNAs coding for human putative OBPs have been reported to be also expressed in the genital sphere (*34*).

Among tested odorants, $hOBP_{IIa\alpha}$ was shown to strongly interact with aldehydes, but exhibits a 20-fold weaker affinity for some odorants such as eugenol. This suggests that a set of complementary OBPs with different specificity, as reported for rat OBP subtypes (*27*), would be necessary to solubilize a vast array of diverse odorants, which are perceived by human beings. Alternative splicing of OBP genes, described in human species (*34*), could be involved in generating such OBP variants. Moreover, heterologous expression of hOBP opens the possibility for site-directed mutagenesis of specific residues, such as lysines, to investigate the relationships between the structure and the function of human OBPs.

ACKNOWLEDGMENT

We are grateful to Dr. Alain Zachowski for helpful discussion and to Dominique Le Bars for its kind assistance. We also want to thank Floressence (Courbevoie, France), Givaudan-Roure (Allauch, France), International Flavors and Fragrances (Dijon, France), and SKW Biosystems (Grasse, France) for their precious gifts of numerous odorants.

REFERENCES

1. Steinbrecht, R. A. (1998) *Ann. New York Acad. Sci. 855*, 323−332.
2. Pelosi, P. (1996) *J. Neurobiol. 30*, 3−19.
3. Flower, D. R., North, A. C., and Sansom, C. E. (2000) *Biochim. Biophys. Acta 1482*, 9−24.
4. Tegoni, M., Pelosi, P., Vincent, F., Spinelli, S., Campanacci, V., Grolli, S., Ramoni, R., and Cambillau, C. (2000) *Biochim. Biophys. Acta 1482*, 229−240.
5. Bianchet, M. A., Bains, G., Pelosi, P., Pevsner, J., Snyder, S. H., Monaco, H. L., and Amzel, L. M. (1996) *Nat. Struct. Biol. 3*, 934−939.
6. Tegoni, M., Ramoni, R., Bignetti, E., Spinelli, S., and Cambillau, C. (1996) *Nat. Struct. Biol. 3*, 863−867.
7. Spinelli, S., Ramoni, R., Grolli, S., Bonicel, J., Cambillau, C., and Tegoni, M. (1998) *Biochemistry 37*, 7913−7918.
8. Dal Monte, M., Andreini, I., Revoltella, R., and Pelosi, P. (1991) *Comp. Biochem. Physiol. 99*, 445−451.
9. Pes, D., and Pelosi, P. (1995) *Comp. Biochem. Physiol. 112*, 471−479.
10. Pes, D., Dal Monte, M., Ganni, M., and Pelosi, P. (1992) *Comp. Biochem. Physiol. 103*, 1011−1017.
11. Pevsner, J., Trifiletti, R., Strittmatter, S. M., and Snyder, S. H. (1985) *Proc. Natl Acad. Sci. U.S.A. 82*, 3050−3054.
12. Pevsner, J., Reed, R. R., Feinstein, P. G., and Snyder, S. H. (1988) *Science 241*, 336−339.
13. Briand, L., Nespoulous, C., Perez, V, Remy, J.-J., Huet, J.-C., and Pernollet, J.-C. (2000) *Eur. J. Biochem. 267*, 3079−3089.
14. Bignetti, E., Cavaggioni, A., Pelosi, P., Persaud, K. C., Sorbi, R. T., and Tirindelli, R. (1985) *Eur. J. Biochem. 149*, 227−231.
15. Pelosi, P., Baldaccini, E., and Pisanelli, A. M. (1982) *Biochem. J. 201*, 245−248.
16. Scaloni, A., Paolini, S., Brandazza, A., Fantacci, M., Bottiglieri, C., Marchese, S., Navarrini, A., Fini, C., Ferrara, L., and Pelosi, P. (2001) *Cell Mol. Life Sci. 58*, 823−834.
17. Miyawaki, A., Matsushita, F., Ryo, Y., and Mikoshiba, K. (1994) *EMBO J. 13*, 5835−5842.
18. Pes, D., Mameli, M., Andreini, I., Krieger, J., Weber, M., Breer, H., and Pelosi, P. (1998) *Gene 212*, 49−55.
19. Utsumi, M., Ohno, K., Kawasaki, Y., Tamura, M., Kubo, T., and Tohyama, M. (1999) *J. Neurobiol. 39*, 227−236.
20. Dear, T. N., Boehm, T., Keverne, E. B., and Rabbitts, T. H. (1991) *EMBO J. 105*, 775−784.
21. Dear, T. N., Campbell, K., and Rabbitts, T. H. (1991) *Biochemistry 30*, 10376−10382.

22. Ohno, K., Kawasaki, Y., Kubo, T., and Tohyama, M. (1996) *Neuroscience 71*, 355−366.
23. Löbel, D., Strotmann, J., Jacob M., and Breer, H. (2001) *Chem. Senses 26*, 673−80.
24. Garibotti, M., Navarrini, A., Pisanelli, A. M., and Pelosi, P. (1997) *Chem. Senses 22*, 383−390.
25. Felicioli, A., Ganni, M., Garibotti, M., and Pelosi, P. (1993) *Comp. Biochem. Physiol. 105*, 775−784.
26. Ganni, M., Garibotti, M., Scaloni, A., Pucci, P., and Pelosi, P. (1997) *Comp. Biochem. Physiol. 117B*, 287−291.
27. Löbel, D., Jacob, M., Völkner, M., and Breer, H. (2002) *Chem. Senses 27*, 39−44.
28. Löbel, D., Marchese, S., Krieger, J., Pelosi, P., and Breer, H. (1998) *Eur. J. Biochem. 254*, 318−324.
29. Maremmani, C., Fattori, B., De Ciccio, M., Ceravolo, R., Ghilardi, P. L., and Muratorio, A. (1996) *Rhinology 34*, 147−150.
30. Scalfari, F., Castagna, M., Fattori, B., Andreini, I., Maremmani, C., and Pelosi, P. (1997) *Comp. Biochem. Physiol. 118B*, 819−824.
31. Lindahl, M., Stahlbom B., and Tagesson, C. (1999) *Electrophoresis 20*, 3670−3676.
32. Lindahl, M., Stahlbom, B., and Tagesson, C. (2001) *Electrophoresis 22*, 1795−1800.
33. Burkhard, P. R., Rodrigo, N., May, D., Sztajzel, R., Sanchez, J. C., Hochstrasser, D. F., Shiffer, E., Reverdin, A., and Lacroix, J. S. (2001) *Electrophoresis 22*, 1826−1833.
34. Lacazette E., Gachon A. M., and Pitiot, G. (2000) *Hum. Mol. Genet. 9*, 289−301.
35. Lang, J. (1989) *Clinical Anatomy of the Nose, Nasal Cavity and Paranasal Sinuses*, Thieme Medical Publishers, New York, USA.
36. Sallantin, M., Huet, J.-C., Demarteau, C., and Pernollet, J.-C. (1990) *Electrophoresis 11*, 34−36.
37. Briand, L., Nespoulous, C., Huet, J.-C., Takahashi, M., and Pernollet, J.-C. (2001) *Eur. J. Biochem. 268*, 752−760.
38. Pace, C. N., Vajdos, F., Fee, L., Grimsley, G., and Gray, T. (1995) *Protein Sci. 4*, 2411−2423.
39. Deleage, G., and Geourjon, C. (1993) *Comput. Applic. Biosci. 9*, 87−91.
40. Briand, L, Huet, J.-C., Perez, V., Lenoir, G., Nespoulous, C., Boucher, Y., Trotier, D., and Pernollet, J.-C. (2000) *FEBS Lett. 476*, 179−185.
41. Norris, A. W., and Li, E. (1998) In *Retinoid Protocols* (Redfern, C. P. F., Ed) *Methods in Molecular Biology*, Vol 89, pp 123−139, Humana Press Inc., Totowa, NJ.
42. Ramoni, R., Vincent, F., Grolli, S., Conti, V., Malosse, C., Boyer, F. D., Nagnan-Le Meillour, P., Spinelli, S., Cambillau, C., and Tegoni, M. (2001) *J. Biol. Chem. 276*, 7150−7155.
43. Guex, N., and Peitsch, M. C. (1997) *Electrophoresis 18*, 2714−2723.
44. Wojnar, P., Lechner, M., Merschak, P., and Redl, B. (2001) *J. Biol. Chem. 276*, 20206−20212.
45. Tanaka, T., Urade, Y., Kimura, H., Eguchi, N., Nishikawa, A., and Hayaishi, O. (1997) *J. Biol. Chem. 272*, 15789−15795.
46. Muresan, S., van Der Bent, A., and de Wolf, F. A. (2001) *J. Agric. Food Chem. 49*, 2609−2618.
47. Jain, M. K., and Maliwal, B. P. (1985) *Biochim. Biophys. Acta 814*, 135−140.
48. de Foresta, B., Champeil, P., and le Maire, M. (1990) *Eur. J. Biochem. 194*, 383−388.
49. Mei, B., Kennedy, M. W., Beauchamp, J., Komuniecki, P. R., and Komuniecki, R. (1997) *J. Biol. Chem. 272*, 9933−9941.
50. Lechner, M., Wojnar, P., and Redl, B. (2001) *Biochem. J. 356*, 129−135.
51. Paolini, S., Marchese, S., Scaloni, A., and Pelosi, P. (1998) *Chem. Senses 23*, 689−698.
52. Marie, D. A., Veggerby, C., Robertson, D. H., Gaskell, S. J., Hubbard, S. J., Martinsen, L., Hurst, J. L., and Beynon, R. J. (2001) *Protein Sci. 10*, 411−417.
53. Ghafouri, B., Stahlbom, B., Tagesson, C., and Lindahl, M. (2002) *Proteomics 2*, 112−120.
54. Morison, E. E., and Moran, D. T. (1995) In *Handbook of Olfaction and Gustation* (Doty, R. L., Ed.) pp 75−101, Marcel Dekker, New York, USA.
55. Leopolds, D. A., Hummel, T., Schwob, J. E., Chen Hong, S., Knecht, M., and Kobal, G. (2000) *Laryngoscope 110*, 417−421.
56. Pevsner, J., Hwang, P. M., Sklar, P. B., Venable, J. C., and Snyder, S. H. (1988) *Proc. Natl. Acad. Sci. U.S.A. 85*, 2383−2387.
57. Böcskei, Z., Groom, C. R., Flower, D. R., Wright, C. E., Phillips, S. E. V., Cavaggioni, A., Findlay, J. B. C., and North, A. C. T. (1992) *Nature 360*, 186−188.
58. van't Hof, W. V., Blankenvoorde, M. F. J., Veerman, E. C. I., and Amerongen, A. V. (1997) *J. Biol. Chem. 272*, 1837−1841.
59. Suire, S., Stewart, F., Beauchamp, J., and Kennedy, M. W. (2001) *Biochem. J. 356*, 369−376.
60. Macgregor, R. B., and Weber, G. (1986) *Nature 319*, 70−73.
61. Guerbette, F., Grosbois, M., Jolliot-Croquin, A., Kader, J.-C., and Zachowski, A. (1999) *Biochemistry 48*, 14131−14137.
62. Vincent, F., Spinelli, S., Ramoni R., Grolli, S., Pelosi, P., Cambillau, C., and Tegoni, M. (2000) *J. Mol. Biol. 300*, 127−139.
63. Cho, Y., Batt, C. A, and Sawyer, L. (1994) *J. Biol. Chem. 269*, 11102−11107.
64. Paolini, S., Tanfani, F., Fini, C., Bertoli, E., and Pelosi, P. (1999) *Biochim. Biophys. Acta 23*, 689−698.
65. Yusifov, T. N., Abduragimov, A. R., Gasymov, O. K., and Glasgow, B. J. (2000) *Biochem. J. 347*, 815−819.

BI015916C